Activating Multistep Charge-Transfer Processes in Fullerene–Subphthalocyanine–Ferrocene Molecular Hybrids as a Function of π–π Orbital Overlap

ARTICLE *in* JOURNAL OF THE AMERICAN CHEMICAL SOCIETY · OCTOBER 2010

Impact Factor: 12.11 · DOI: 10.1021/ja105864r · Source: PubMed

6 AUTHORS, INCLUDING:

Esther Carbonell
University of Valencia
35 PUBLICATIONS **967** CITATIONS
SEE PROFILE

Gustavo de Miguel Rojas
University of Cordoba (Spain)
34 PUBLICATIONS **572** CITATIONS
SEE PROFILE

Carmen Atienza
Complutense University of Madrid
39 PUBLICATIONS **1,025** CITATIONS
SEE PROFILE

J|A|C|S ARTICLES

Published on Web 10/29/2010

Activating Multistep Charge-Transfer Processes in Fullerene−Subphthalocyanine−Ferrocene Molecular Hybrids as a Function of $\pi-\pi$ Orbital Overlap

David González-Rodríguez,[‡] Esther Carbonell,[§] Gustavo de Miguel Rojas,[§] Carmen Atienza Castellanos,[§] Dirk M. Guldi,[§,*] and Tomás Torres[‡,⊥,*]

Departamento de Química Orgánica, Facultad de Ciencias, Universidad Autónoma de Madrid, E-28049 Madrid, Spain, Department of Chemistry and Pharmacy and Interdisciplinary Center for Molecular Materials (ICMM), Friedrich-Alexander-Universität Erlangen-Nürnberg, 91058 Erlangen, Germany, and IMDEA-Nanociencia, Facultad de Ciencias, Ciudad Universitaria de Cantoblanco, 28049 Madrid, Spain

Received July 8, 2010; E-mail: dirk.guldi@chemie.uni-erlangen.de; tomas.torres@uam.es

Abstract: We have synthesized two different fullerene−subphthalocyanine−ferrocene conjugates. The molecules were designed so that the ferrocene unit is linked at the subphthalocyanine axial position through a phenoxy spacer while the C_{60} is rigidly held close to the concave face of the macrocycle via a 3-fold C_3-symmetrical anchoring. The Bingel trisaddition reaction leading to the final products proceeded with very high regioselectivities and full diastereoselectivity. The only difference between both systems is the length of the triple tether employed, which finely regulates the regioselectivity of the trisaddition reaction and the distance between the subphthalocyanine and the C_{60} complementary $\pi-\pi$ surfaces. Thus, when the tether is connected to the subphthalocyanine through a direct C−C bond, a short $\pi-\pi$ distance of 3.25−3.30 Å was calculated. In contrast, when it is connected through a slightly longer C−O−C bond, the distance increases to 3.5−3.6 Å. This $\pi-\pi$ distance has a strong influence on the ground-state electronic interactions between the subphthalocyanine and the C_{60}, as determined from electronic absorption and cyclic voltammetry measurements. In addition, fluorescence and time-resolved transient absorption experiments demonstrated that different mechanisms operate in the two systems after photoexcitation. Despite the similar HOMO−LUMO gaps, only when the two complementary $\pi-\pi$ surfaces of the subphthalocyanine and the C_{60} are held at a close distance, therefore showing a high degree of orbital overlap, is a multistep electron transfer process triggered, ultimately leading to the long-lived, spatially separated C_{60} radical anion and ferrocenium radical cation pair. A full account of the synthesis, characterization, and studies of the ground- and excited-state electronic interactions occurring in these conjugates, as well as in their reference C_{60}−subphthalocyanine and subphthalocyanine−ferrocene dyads, is presented in this article.

Introduction

Understanding and controlling multistep electron transfer processes at the molecular level, as mastered by natural photosynthetic systems,[1] is considered to be fundamental for the development of efficient organic solar energy conversion systems.[2] The basic concept relies on promoting sequential electron transfer reactions between π-conjugated, electronically active units, properly arranged following a redox gradient, that ultimately leads to spatially separated radical ion pairs.[3] Although the resulting charge-separated state usually exhibits attenuated electronic couplings and therefore prolonged lifetimes, a major drawback of this strategy is the substantial loss of input energy in each electron transfer step. In order to minimize this energy loss, a proper compromise between the redox gradients and the electronic couplings between the different active units must be reached.[4]

The degree of electronic interaction between the different molecules in these multicomponent systems, regulated by their relative distance, orientation, and the nature of the linkages between them, therefore arises as one of the most important parameters that influence the kinetics of the mechanisms that are triggered after photoexcitation.[5] While a number of studies have already underlined the role of the degree of electronic

[‡] Universidad Autónoma de Madrid.
[§] Friedrich-Alexander-Universität Erlangen-Nürnberg.
[⊥] IMDEA-Nanociencia.

(1) (a) *Molecular Mechanisms of Photosynthesis*; Blankenship, R. E., Ed.; Blackwell Science: Malden, MA, 2002. (b) Melkozernov, A. N.; Barber, J.; Blankenship, R. E. *Biochemistry* **2006**, 331–345.
(2) (a) Winder, C.; Sariciftci, N. S. *J. Mater. Chem.* **2004**, *14*, 1077–1086. (b) Guenes, S.; Neugebauer, H.; Sariciftci, N. S. *Chem. Rev.* **2007**, *107*, 1324–1338.
(3) (a) Imahori, H.; Tamaki, K.; Araki, Y.; Sekiguchi, Y.; Ito, O.; Sakata, Y.; Fukuzumi, S. *J. Am. Chem. Soc.* **2002**, *124*, 5165–5174. (b) Springer, J.; Kodis, G.; De La Garza, L.; Moore, A. L.; Moore, T. A.; Gust, D. *J. Phys. Chem. A* **2003**, *107*, 3567–3575. (c) D'Souza, F.; Chitta, R.; Gadde, S.; Islam, D.-M. S.; Schumacher, A. L.; Zandler, M. E.; Araki, Y.; Ito, O. *J. Phys. Chem. B* **2006**, *110*, 25240–25250. (d) González-Rodríguez, D.; Bottari, G. *J. Porphyrins Phthalocyanines* **2009**, *13*, 624–636.
(4) Imahori, H.; Mori, Y.; Matano, Y. *J. Photochem. Photobiol. C* **2003**, *4*, 51–83.

 10.1021/ja105864r

coupling in multicomponent systems in solution,[6] one can expect that the effects of this parameter are even more critical in solid-state photovoltaic devices.[2] In fact, in the absence of a solvent medium, the π-conjugated photoactive molecules are forced to pack via intimate van der Waals interactions and conformational or orientational motions are severely limited. Most of the synthetic donor−acceptor models described so far fail to reproduce this situation where, due a higher degree of orbital overlap between the confined molecules, the fate of the harvested energy may be controlled by mechanisms different to those operating in molecularly dissolved systems.

We and others have previously demonstrated that covalent systems that combine subphthalocyanine (SubPc)[7] and C_{60} fullerene do not exhibit a large driving force for photoinduced charge separation. Despite the relatively high excitation energy of SubPcs (ca. 2.1 eV), these macrocycles typically exhibit high or moderate oxidation potentials, which results in a high-energy $SubPc^{\bullet+}-C_{60}^{\bullet-}$ charge-separated state. Instead, energy transfer processes arise as the dominant mechanism operating after photoexcitation.[8] Only when the SubPc core is substituted with strong electron-donating groups at the periphery (i.e., amines), thereby lowering its oxidation potential, are electron transfer processes observed in these SubPc−C_{60} hybrids.[8b,f] So far this has been proven in weakly coupled conjugates, where the SubPc axial position served to connect C_{60} through partially conjugated spacers.

However, we recently described C_{60}−SubPc capped conjugates where electron transfer can compete with energy transfer mechanisms due to an intimate $\pi-\pi$ contact between the two photoactive units.[9] Here, we profit from the synthetic versatility of SubPcs and coupled an additional ferrocene (Fc) electron-donating unit at the axial position of the macrocycle. In these C_{60}−SubPc−Fc the SubPc light-harvesting unit is situated between the acceptor and the donor moieties and can thus mediate their electronic communication. We show that multistep charge-transfer mechanisms, ultimately leading to the spatially separated $C_{60}^{\bullet-}-SubPc-Fc^{\bullet+}$ radical ion pair, are only triggered when the C_{60} and the SubPc chromophores are rigidly maintained at a short distance and forced to strongly interact through their complementary curved π-surfaces.[10] This $\pi-\pi$ distance, and hence the degree of orbital overlap, could be finely adjusted by just varying the linkage between the three semirigid spacers that anchor the SubPc to the C_{60}: a shorter C−C bond (***-C*** series) or a slightly longer C−O−C bond (***-O*** series). A full account of the synthesis, characterization, and our studies of the ground- and excited-state electronic interactions occurring in these C_{60}−SubPc−Fc systems, as well as in their respective C_{60}−SubPc and SubPc−Fc reference compounds, is presented in this article.

Results and Discussion

Synthesis. Two different synthetic routes to the SubPc−Fc conjugates (**S-Fc**), C_{60}−SubPc (**C_{60}-S**) conjugates, and C_{60}−SubPc−Fc (**C_{60}-S-Fc**) conjugates were designed, depending on the connection of the spacer to the SubPc macrocycle: a direct C−C bond (***-C*** series) or an oxygen atom (***-O*** series).

The compounds of the ***-C*** series (Scheme 1) were prepared starting from a chloro-SubPc peripherally substituted with three iodine atoms (**3**),[11] which was synthesized by cyclotrimerization reaction of 4-iodophthalonitrile (**4**) in the presence of BCl_3.[12] The axial chlorine atom in **3** was then replaced either by 4-*tert*-octylphenol or 4-ferrocenylphenol, leading respectively, after chromatographic separation of the 1:3 mixture of C_3/C_1 regioisomers, to SubPcs **2-*C*** and **2-Fc-*C***. These compounds were then subjected to a Suzuki reaction with (2-hydroxyphenyl)pinacol boronate,[13] affording trihydroxy derivatives **1-*C*** and **1-Fc-*C*** in good yields. Finally, the acylation reaction between **1-*C*** or **1-Fc-*C*** and ethyl malonyl chloride led to SubPc **S-*C*** and SubPc−Fc dyad **S-Fc-*C***, respectively.

On the other hand, the route leading to the products in the ***-O*** series (Scheme 2) starts with the condensation reaction of the TBDMS-protected phthalonitrile **6**. The silylether groups in this reagent are sufficiently stable to resist the harsh conditions of the cyclotrimerization reaction with BCl_3. It is known that chloro-SubPcs that are peripherally functionalized with electron-donating groups can easily undergo axial exchange reactions.[7b] Therefore, in order to avoid the formation of the corresponding axially hydroxy-substituted SubPc during chromatographic workup, we decided to carry out the axial replacement of the chlorine atom with the phenol derivatives just after the condensation reaction, without isolation of the corresponding chloro-SubPcs. This led to compounds **5-*O*** and **5-Fc-*O***, which are axially equipped with 4-*tert*-octylphenoxy and 4-ferrocenylphenoxy units, respectively. Deprotection of the TBDMS groups in **5-*O*** and **5-Fc-*O*** in the presence of TBAF[13a] led to the corresponding trihydroxy SubPcs **1-*O*** and **1-Fc-*O***. As we did with SubPcs **1-*C*** and **1-Fc-*C***, compounds **1-*O*** and **1-Fc-*O*** were finally subjected to an acylation reaction with ethyl malonyl chloride, yielding SubPc **S-*O*** and SubPc−Fc dyad **S-Fc-*O***, respectively. The isolation of the C_3 regioisomer was carried

(5) (a) Guldi, D. M.; Hirsch, A.; Scheloske, M.; Dietel, E.; Troisi, A.; Zerbetto, F.; Prato, M. *Chem.—Eur. J.* **2003**, *9*, 4968–4979. (b) Albinsson, B.; Eng, M. P.; Pettersson, K.; Winters, M. U. *Phys. Chem. Chem. Phys.* **2007**, 5847–5864. (c) Araki, Y.; Ito, O. *J. Photochem. Photobiol. C* **2008**, *9*, 93–110.
(6) (a) El-Khouly, M. E.; Ito, O.; Smith, P. M.; D'Souza, F. *J. Photochem. Photobiol., C* **2004**, *5*, 79–104. (b) Fukuzumi, S. *Phys. Chem. Chem. Phys.* **2008**, *10*, 2283–2297. (c) D'Souza, F.; Ito, O. *Organic Electronics and Photonics*; Nalwa, H. R., Ed.; American Scientific Publishers: Stevenson Ranch, CA, 2008; Vol. 1, Chap. 13. (d) Ohkubo, K.; Fukuzumi, S. *Bull. Chem. Soc. Jpn.* **2009**, *82*, 303–315.
(7) (a) *The Porphyrin Handbook*; Kadish, K. M., Smith, K. M., Guillard, R., Eds.; Academic Press: San Diego, 2003; Vol. 15. (b) Claessens, C. G.; González-Rodríguez, D.; Torres, T. *Chem. Rev.* **2002**, *102*, 835–853. (c) Torres, T. *Angew. Chem., Int. Ed.* **2006**, *45*, 2834–2837. (d) Claessens, C. G.; Medina, A. *J. Porphyrins Phthalocyanines* **2009**, *13*, 446–454.
(8) (a) González-Rodríguez, D.; Torres, T.; Guldi, D. M.; Rivera, J.; Echegoyen, L. *Org. Lett.* **2002**, *4*, 335–338. (b) González-Rodríguez, D.; Torres, T.; Guldi, D. M.; Rivera, J.; Herranz, M. A.; Echegoyen, L. *J. Am. Chem. Soc.* **2004**, *126*, 6301–6313. (c) Iglesias, R. S.; Claessens, C. G.; Torres, T.; Rahman, G. M. A.; Guldi, D. M. *Chem. Commun.* **2005**, 2113–2115. (d) Iglesias, R. S.; Claessens, C. G.; Rahman, G. M. A.; Herranz, M. A.; Guldi, D. M.; Torres, T. *Tetrahedron* **2007**, *63*, 12396–12404. (e) Kim, J.-H.; El-Khouly, M. E.; Araki, Y.; Ito, O.; Kay, K.-Y. *Chem. Lett.* **2008**, *37*, 544–545. (f) González-Rodríguez, D.; Torres, T.; Herranz, M. A.; Echegoyen, L.; Carbonell, E.; Guldi, D. M. *Chem.—Eur. J.* **2008**, *14*, 7670–7679.
(9) González-Rodríguez, D.; Carbonell, E.; Guldi, D. M.; Torres, T. *Angew. Chem., Int. Ed.* **2009**, *48*, 8032–8036.
(10) (a) Giaimo, J. M.; Gusev, A. V.; Wasielewski, M. R. *J. Am. Chem. Soc.* **2002**, *124*, 8530–8531. (b) Veldman, D.; Chopin, S. M. A.; Meskers, S. C. J.; Groeneveld, M. M.; Williams, R. M.; Janssen, R. A. J. *J. Phys. Chem. A* **2008**, *112*, 5846–5857. (c) Giaimo, J. M.; Lockard, J. V.; Sinks, L. E.; Scott, A. M.; Wilson, T. M.; Wasielewski, M. R. *J. Phys. Chem. A* **2008**, *112*, 2322–2330.
(11) Claessens, C. G.; Torres, T. *Tetrahedron Lett.* **2000**, *41*, 6361–6365.
(12) Claessens, C. G.; González-Rodríguez, D.; del Rey, B.; Torres, T.; Mark, G.; Schuchmann, H.-P.; von Sonntag, C.; MacDonald, J. G.; Nohr, R. S. *Eur. J. Org. Chem.* **2003**, 2547–2551.
(13) (a) González-Rodríguez, D.; Torres, T. *Eur. J. Org. Chem.* **2009**, 1871–1879. (b) González-Rodríguez, D.; Martínez-Díaz, M. V.; Abel, J.; Echegoyen, L.; Perl, A.; Huskens, J.; Torres, T. *Org. Lett.* **2010**, *12*, 2970–2973.

Scheme 1. Synthetic Route to C_{60}−SubPc−Fc **C_{60}-S-Fc-*C***, SubPc−Fc **S-Fc-*C***, C_{60}−SubPc **C_{60}-S-*C***, and Reference SubPc **S-*C***[a]

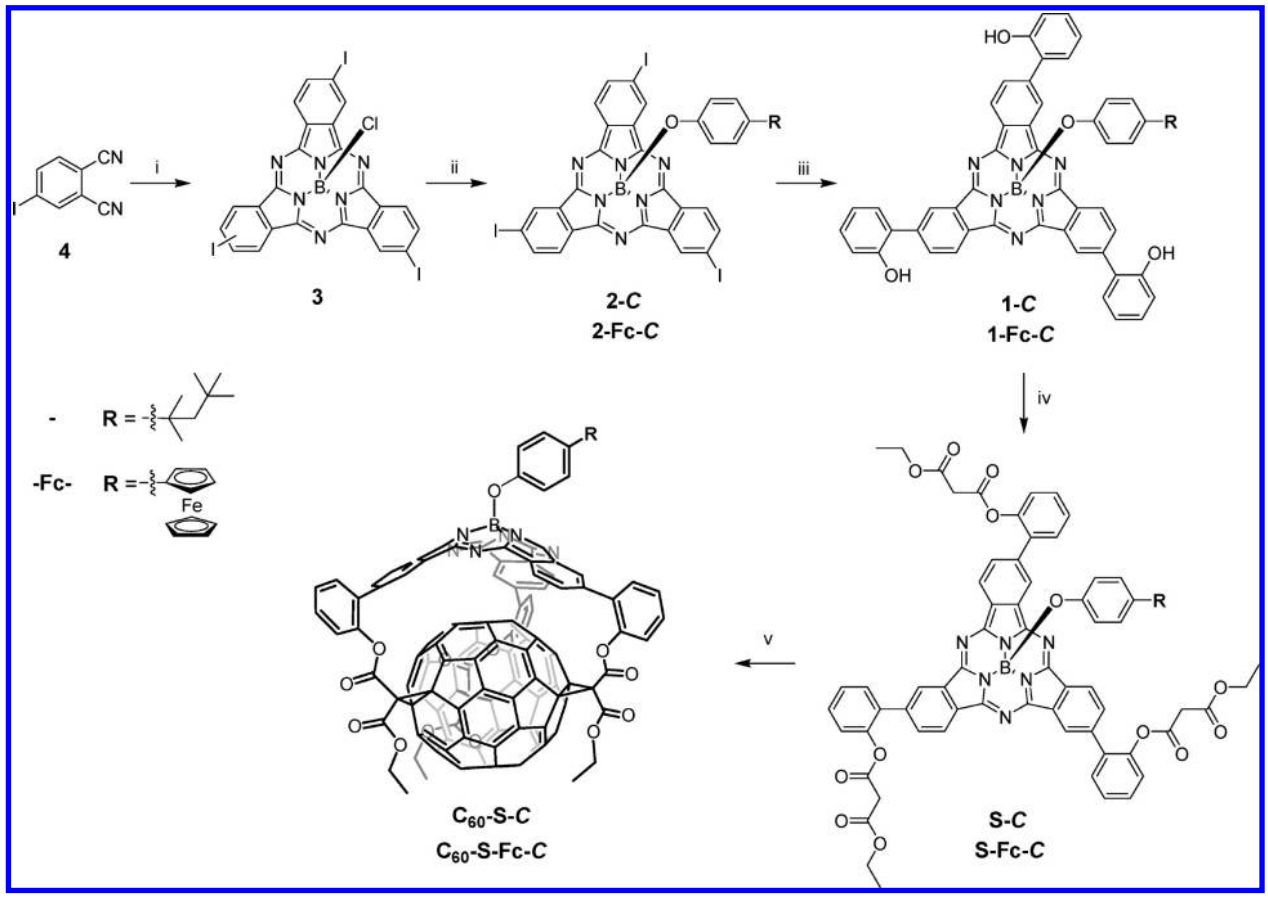

[a] (i) BCl_3, *p*-xylene; (ii) a) 4-*tert*-octylphenol (for **2-*C***) or 4-ferrocenylphenol (for **2-Fc-*C***), toluene; (b) chromatographic isolation of the SubPc C_3-regioisomer; (iii) (2-hydroxyphenyl)pinacol boronate, $Pd(PPh_3)_4$, CsF, DME; (iv) ethyl malonyl chloride, DMAP, THF; (v) C_{60}, I_2, DBU, toluene.

out at this stage mainly due to a better separation in silica gel compared with the regiosomeric mixtures of the previous intermediates.

The coupling of the ethyl malonyl-functionalized, C_3-symmetrical SubPcs **S-*C***, **S-Fc-*C***, **S-*O***, and **S-Fc-*O*** with C_{60} fullerene was performed via a triscyclopropanation reaction in the presence of DBU and I_2.[14] The reaction was carried out under high dilution conditions ($\sim 5 \times 10^{-4}$ M), to avoid undesired multifullerenic products, and at different temperatures (between −10 and 40 °C), in order to assess any temperature effects on the trisaddition pattern (see below).[15] The trisaddition process was completed within a few minutes, leading to C_{60}−SubPc conjugates **C_{60}-S-*C*** and **C_{60}-S-*O***, and C_{60}−SubPc−Fc conjugates **C_{60}-S-Fc-*C*** and **C_{60}-S-Fc-*O***, having respectively a direct C−C bond or an oxygen atom connecting the SubPc and the spacer. The yields obtained in this last step vary considerably, depending on this connection. Whereas **C_{60}-S-*C*** and **C_{60}-S-Fc-*C*** are formed in 80−60% yield at different temperatures, **C_{60}-S-*O*** and **C_{60}-S-Fc-*O*** could only be obtained in 40−25% yield.[16] All compounds were purified and characterized by ^{1}H and ^{13}C NMR techniques, LSI or MALDI-TOF mass spectrometry, and UV−vis and IR spectroscopies.[15]

Trisadduct Characterization. The nature of the axial ligand (i.e., 4-*tert*-octylphenoxy or 4-ferrocenylphenoxy) has, as expected, no influence on the trisaddition pattern obtained. Therefore the triscyclopropanation reactions leading to **C_{60}-S-*C*/C_{60}-S-Fc-*C*** and to **C_{60}-S-*O*/C_{60}-S-Fc-*O*** were found to proceed with the same regio- and diastereoselectivity for each tether. In order to ascertain the binding patterns to the fullerene in the trisadducts, we studied the products by NMR spectroscopy (^{1}H, ^{13}C, HMQC and NOESY NMR) and performed molecular modeling studies using a combination of semiempirical (PM3) and density functional theory (DFT; B3LYP/3-21G) methods.[15]

When the linker is connected to the SubPc macrocycle via a C−C bond (**-*C*** series), the trisaddition reaction between **S-Fc-*C*** or **S-*C*** and C_{60} at 20 °C yields a 5:95 mixture of two regioisomers (**α** and ***β***, respectively; Figures 1, and Figures S1−S4, Supporting Information) that could be separated by successive flash column chromatographies. The main component of these mixtures, **C_{60}-S-Fc-*Cβ*/C_{60}-S-*Cβ***, presents three set of signals for each proton/carbon in the ^{1}H and ^{13}C NMR spectra,[15] respectively, and therefore has C_1 symmetry (Figure 1a). On the other hand, the minor component, **C_{60}-S-Fc-*C*α/C_{60}-S-*C*α**, retains the same C_3 symmetry of the precursor SubPc (**S-Fc-*C*/S-*C***; Figure 1b).

We assigned compounds **C_{60}-S-Fc-*C*α** and **C_{60}-S-*C*α** to the *t3,t3,t3* trisadducts. The other three possible C_3-symmetrical trisaddition patterns to C_{60} (*c1,c1,c1*, *e,e,e*, and *t4,t4,t4*)[17] were discarded since they would lead to rather constrained structures (imposed by the rigid nature of the SubPc core and the restricted

(14) Bingel, C. *Chem. Ber.* **1993**, *126*, 1957–1959.
(15) Please, see the Supporting Information for further details.
(16) The reason for this fact actually comes from the particular instability of the malonate−SubPcs in the **-*O*** series under slightly warm and acidic conditions, where partial hydrolysis, leading to hydroxy-substituted compounds, is very difficult to avoid, and we always observed a polar residue during chromatographic purification.

Scheme 2. Synthetic Route to C_{60}−SubPc−Fc **C_{60}-S-Fc-*O***, SubPc−Fc **S-Fc-*O***, C_{60}−SubPc **C_{60}-S-*O***, and Reference SubPc **S-*O***[a]

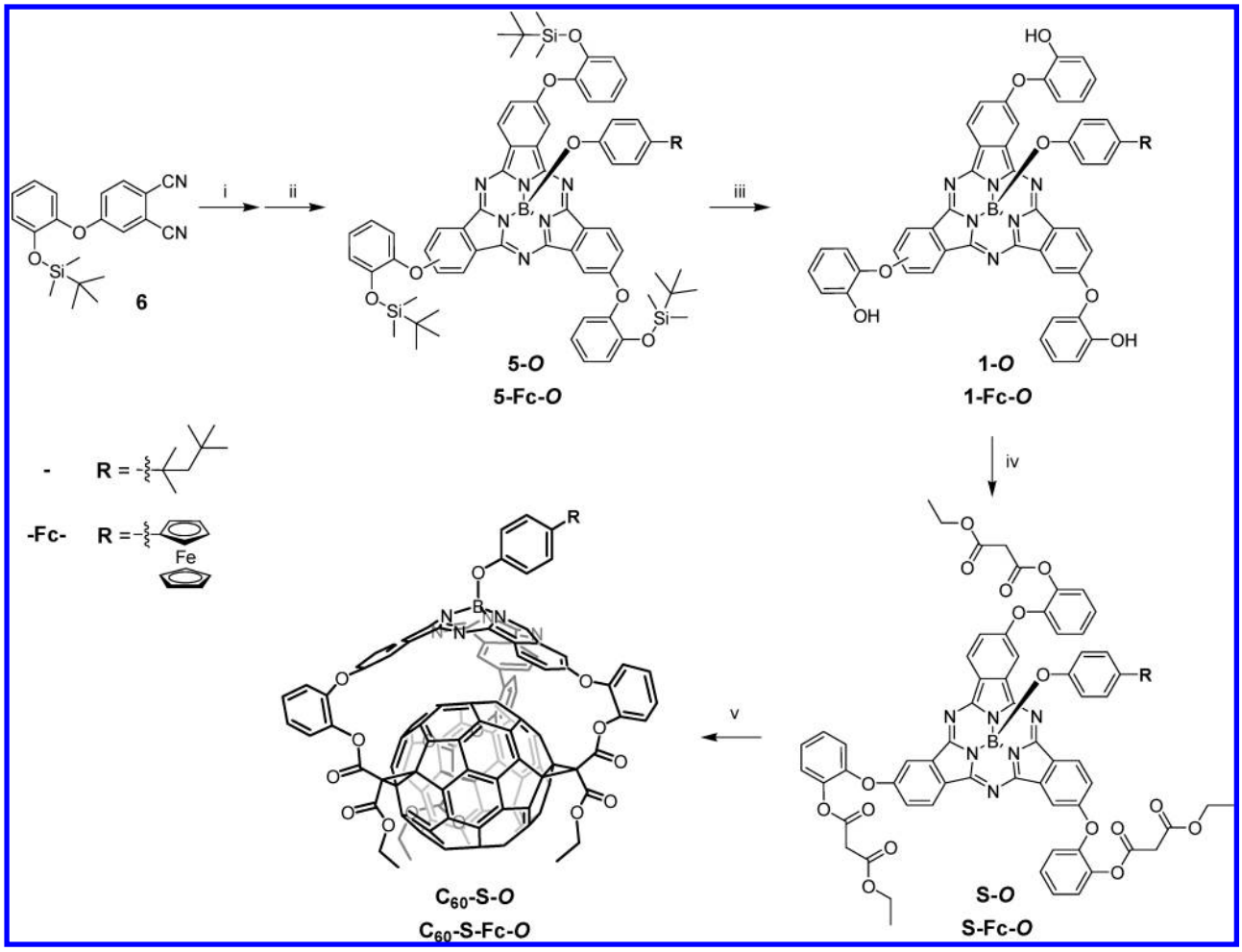

[a] (i) BCl_3, *p*-xylene; (ii) 4-*tert*-octylphenol (for **5-*O***) or 4-ferrocenylphenol (for **5-Fc-*O***), toluene; (iii) Bu_4NF, THF; (iv) (a) ethyl malonyl chloride, DMAP, THF; (b) chromatographic isolation of the SubPc C_3-regioisomer; (v) C_{60}, I_2, DBU, toluene.

flexibility of the spacers used) due to the smaller spacing between the cyclopropane rings. This is immediately obvious for the *c1,c1,c1* and *e,e,e* patterns, so only the relative stabilities of the *t3,t3,t3* and *t4,t4,t4* isomers were analyzed in detail. The relative single point energies of up to five optimized structures,[15] having different spacer conformations, for each of the two possible diastereoisomers of both the *t3,t3,t3* and *t4,t4,t4* trisadducts were evaluated making use of semiempirical (PM3) and density functional theory (DFT; B3LYP/3-21G) methods. The results (Figure S17, Supporting Information) clearly indicated that the *t3,t3,t3* isomers are much more stable than the *t4,t4,t4* trisadducts.[18] In addition to being thermodynamically less stable, the formation of a *t4,t4,t4* trisadduct is, in general, kinetically unfavorable due to electronic effects.[19]

The binding pattern of the C_1-symmetric **C_{60}-S-Fc-*Cβ*/C_{60}-S-*Cβ*** trisadducts is somewhat more difficult to establish. The formation of only two regioisomers for **C_{60}-S-Fc-*C*** and **C_{60}-S-*C*** seems to indicate that they are structurally related and that the formation of the **α** or ***β*** products is probably decided in the last cyclopropanation step, once the other two malonate groups have been attached to the C_{60} sphere in a *t3* arrangement. The remaining tether (see Figure 1) can then react only with a [6,6] double bond in a *t3* position relative to the other two (leading to the C_3-symmetric *t3,t3,t3* **C_{60}-S-Fc-*Cα*/C_{60}-S-*Cα*** trisadducts), or with one of the two adjacent [6,6] double bonds (yielding **C_{60}-S-Fc-*Cβ*/C_{60}-S-*Cβ***). This leads to the conclusion that the isomers ***β*** must present either a *t3,t2,e* or a *t3,t3,t4* regioisomeric pattern. Careful inspection of the ^{1}H NMR signals of **C_{60}-S-Fc-*Cβ*** and **C_{60}-S-*Cβ*** sustained these hypotheses and helped in the elucidation of the structure of this trisadduct. As shown in Figure 1a, one of the three sets of signals for the aromatic protons ("a", "b", and "c") on the isoindole ring experience marked shifts with respect to the other two. This observation seems to agree with the presence of a biphenyl moiety that presents a different conformation. Of particular importance is the unusual downfield shift (>0.5 ppm) of the proton signal around 9.4 ppm, which may be explained by a spacer conformation in which a carbonyl group of the malonate moiety is close to the a proton of one of the isoindole units (see inset of the

(17) For the sake of simplicity and clarity, we are using the terminology: *c* for *cis*, *e* for *equatorial*, and *t* for *trans*. See: Pasimeni, L.; Hirsch, A.; Lamparth, I.; Maggini, M.; Prato, M. *J. Am. Chem. Soc.* **1997**, *119*, 12902–12905.

(18) A closer inspection to the optimized structures reveals that in the *t4,t4,t4* isomers the rigid SubPc macrocycle is forced to increase significantly its pyramidality (taken as the angle between the perpendicular to the plane of the benzene rings and the B−O axis)[7b] from ∼24° (SubPcB(OPh)) or ∼25−27° (*t3,t3,t3* adducts) to ∼36−40° (*t4,t4,t4* adducts), which may be one of the main reasons for their lower stability.

(19) Chuang, S.-C.; Khan, S. I.; Rubin, Y. *Org. Lett.* **2006**, *8*, 6075–6078.

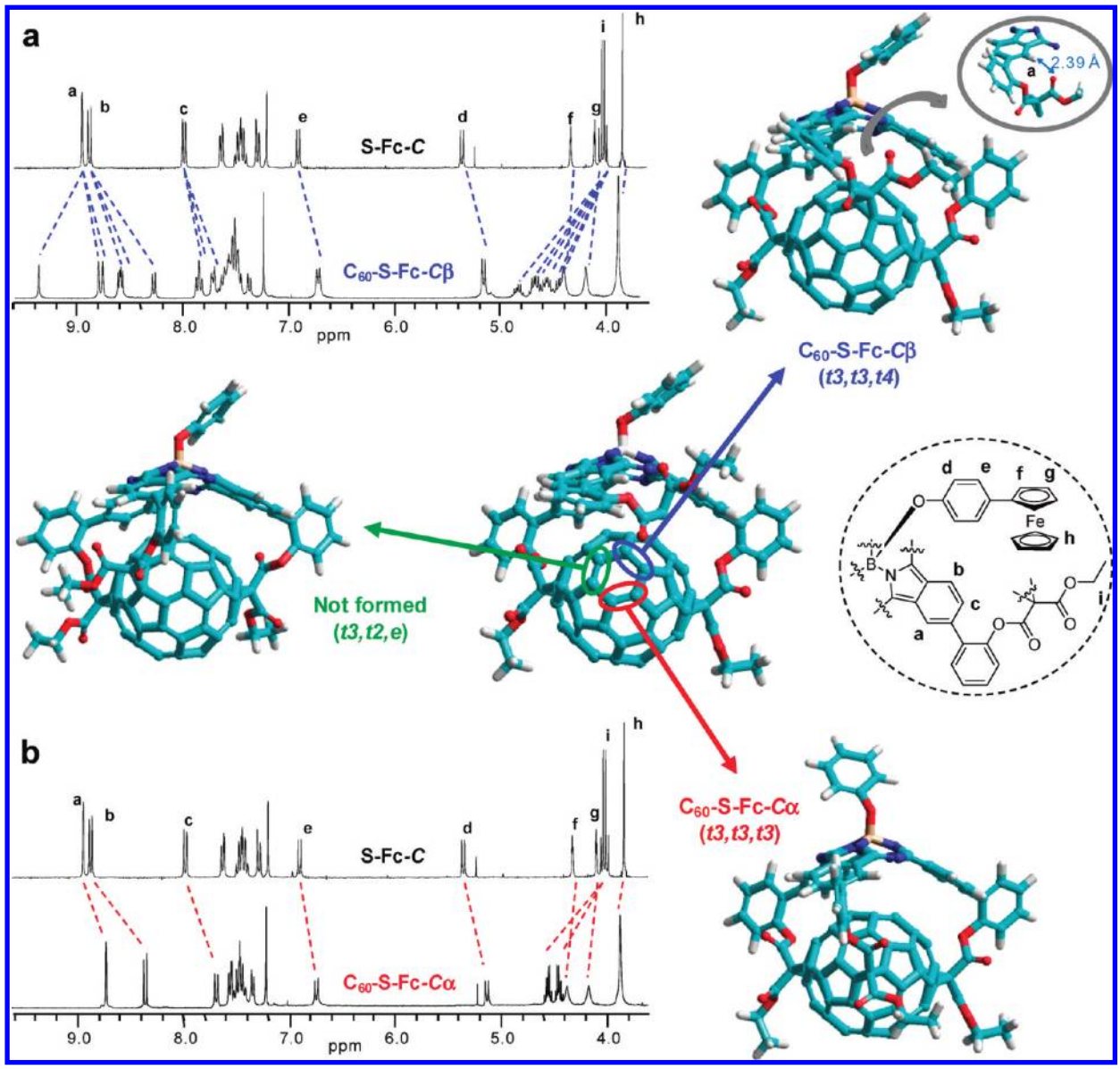

Figure 1. Scheme showing a model of a possible *t3* bisadduct intermediate formed during the triscyclopropanation reaction between **S-Fc-*C*** and C_{60}. The remaining third tether can then react with any of the circled double bonds, yielding the C_3-symmetric *t3,t3,t3* trisadduct (in red; **C_{60}-S-*C*α**), or the C_1-symmetric *t3,t3,t4* (in blue; **C_{60}-S-*Cβ***) or *t3,t2,e* (in green; not formed) trisadducts, whose models are also displayed (the ferrocene unit has been omitted). (a) ^{1}H NMR spectra ($CDCl_3$, 298 K, 500 MHz) of compound **C_{60}-S-Fc-*Cβ*** compared to the **S-Fc-*C*** precursor. The unusual downfield shift of one of the proton "a" signals may be explained by a spacer conformation in which a carbonyl group is close to this isoindole proton, as shown in the magnification of the **C_{60}-S-Fc-*Cβ*** model, which supports our assignment. (b) ^{1}H NMR spectra ($CDCl_3$, 298 K, 500 MHz) of compound **C_{60}-S-Fc-*C*α** compared to the **S-Fc-*C*** precursor.

C_{60}-S-Fc-*Cβ* model in Figure 1a). Interestingly, only some conformers having the *t3,t3,t4* trisadittion pattern can impose such arrangement.

A comparison between the semiempirical- and DFT-calculated relative energies of a collection of conformers and diastereomers for each of the three *t3,t3,t3*, *t3,t2,e*, *t3,t3,t4* **C_{60}-S-*C*** models pointed to an increase in stability in the following order: *t3,t3,t3* < *t3,t2,e* < *t3,t3,t4*, though the energy differences are not very substantial (Figure S17). From the examination of these models, we reasoned that the lower product yields obtained for **C_{60}-S-Fc-*C*α** or **C_{60}-S-*C*α** are due to the rather short SubPc-C_{60} $\pi-\pi$ distances found in the C_3-symmetric *t3,t3,t3* adducts (see below), which would lead to more strained structures and/or transition states. This strain could be partially released by formation of the C_1-symmetrical *t3,t3,t4* trisadduct, which displays slightly longer $\pi-\pi$ distances. Interestingly, we found that the experimental **α/*β*** product ratio was quite sensitive to the reaction temperature and could be altered in favor of the formation of one or the other isomer (see Figure S1). Thus, carrying out the triscyclopropanation reaction at −10 °C resulted in >99% formation of **C_{60}-S-Fc-*Cβ*** or **C_{60}-S-*Cβ***, and a 5:95 mixture of the two regioisomers was instead obtained at 20 °C, while increasing the temperature to 40 °C produced a relative **α/*β*** ratio of 13:87. In view of these results, it seems that the formation of the C_{60} *t3,t3,t3* trisadduct, though usually favored due to symmetry and electronic reasons, only becomes relevant when the **C_{60}-S-Fc-*C*** or **C_{60}-S-*C*** tether is given enough energy to reach the third *t3* position (see Figure 1).

In contrast, when the linker is connected to the SubPc via an oxygen atom, as in **S-Fc-*O*** or **S-*O***, the trisaddition reaction proceeded with quantitative regioselectivity, yielding only one regioisomer (**C_{60}-S-Fc-*O*** or **C_{60}-S-*O***) at all temperatures tested

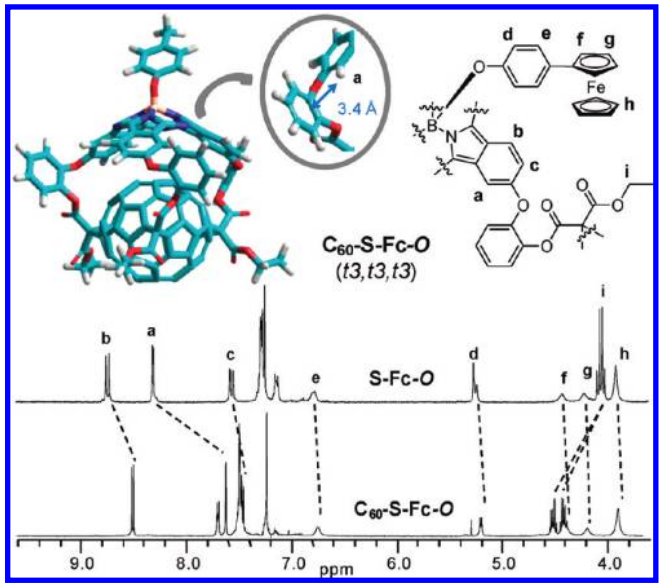

Figure 2. Molecular model and ^{1}H NMR spectra ($CDCl_3$, 298 K, 500 MHz) of compound **C_{60}-S-Fc-*O*** compared to the **S-Fc-*O*** precursor (the ferrocene unit has been omitted). The extraordinary upfield shift of the proton "a" signal could be explained by the conformation adopted by the spacer, as shown in the magnification of the **C_{60}-S-Fc-*O*** model, in which the phenyl group directly faces proton "a".

within the −10−40 °C range. This product shows a single set of signals for each proton/carbon in the NMR spectra (Figure 2) and therefore belongs to the C_3 point group. A *t3,t3,t3* binding pattern was also attributed to compounds **C_{60}-S-Fc-*O*** and **C_{60}-S-*O***, showing again much higher stabilities and less constrained structures than the *t4,t4,t4* isomers (Figure S17).[15] This assignment was further supported by some of the features found in the NMR spectra. For instance, only a *t3,t3,t3* trisaddition pattern is consistent with the exceptional upfield shift experienced by proton "a" in compound **1O** since, due to the conformation adopted by the spacer, it is affected by the aromatic ring current of the nearby phenyl group (Figure 2). HMQC and ^{13}C NMR spectra are also in accordance with this assignment.

In short, these results underscore the subtle role of the tether flexibility and spacing in the regioselectivity of multiple additions to fullerenes.[20−22] A previous comparable approach by the group of Diederich, which uses a more flexible C_3-symmetric cyclotriveratrylene tether, afforded a roughly 1:1 mixture of *t3,t3,t3* and *e,e,e* trisadducts with an overall 20% yield.[23] The regioselectivities observed with our rigid SubPc

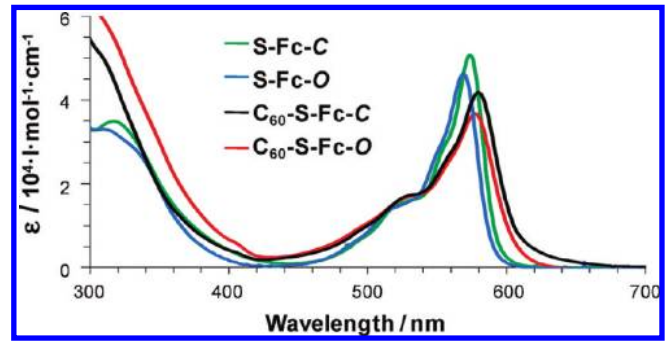

Figure 3. Electronic absorption spectra ($CHCl_3$, $c = 10^{-5}$ M) of **C_{60}-S-Fc-*C*α** and **C_{60}-S-Fc-*O*** compared to SubPc−Fc **S-Fc-*C*** and **S-Fc-*O***.

tether are in contrast remarkable.[24] Compounds **S-Fc-*O*** or **S-*O***, having a phenoxy spacer, seem to meet all the requirements for a fully regioselective trisaddition process to C_{60}, with retention of the SubPc C_3 symmetry. In the case of compounds **S-Fc-*C*** or **S-*C***, the shorter nature of the biphenyl linker restricts the formation of the same C_3, *t3,t3,t3* trisaddition product, and the tether prefers to anchor in a less symmetric arrangement in order to release strain. It is important to remark that these triple addition reactions are not only highly regioselective but also totally diastereoselective, each SubPc enantiomer generating only one enantiomeric addition pattern.[25] The formation of a 1:1 mixture of two enantiomers is clearly evidenced in the splitting of the diastereotopic methylene protons ("i" in Figures 1 and 2) upon trisadduct formation.

Ground-State Studies. Absorption Spectroscopy and Cyclic Voltammetry. The two C_3-symmetric, *t3,t3,t3* C_{60}−SubPc−Fc trisadducts (**C_{60}-S-Fc-*C*α** and **C_{60}-S-Fc-*O***) were further studied by means of diverse ground- and excited-state techniques, along with reference C_{60}−SubPc conjugates (**C_{60}-S-*C*α** and **C_{60}-S-*O***), SubPc−Fc conjugates (**S-Fc-*C*** and **S-Fc-*O***), and reference SubPc (**S-*C*** and **S-*O***), Fc (4-ferrocenylphenol: **FcAr**),[26] and C_{60} (a tris-(diethylmalonate)cyclopropanated fullerene: **C_{60}-m$_3$**)[27] compounds.

It is very relevant to note the differences observed in the DFT-optimized structures (B3LYP; 3-21G*) of compounds **C_{60}-S-Fc-*C*α** and **C_{60}-S-Fc-*O*** with regard to the spacing between the two complementary π-surfaces, which is imposed by the nature of the tether linkage.[15,28] The distances between the two surfaces were estimated as the average value between the six SubPc iminic carbon atoms and the closest atom at C_{60} and fluctuate only slightly with changes in the conformation of the spacer (more evident for compounds having the **-*O*** spacer). As previously described for **C_{60}-S-*C*α** and **C_{60}-S-*O***, in **C_{60}-S-Fc-*C*α**, the concave face of the SubPc is kept in tight van der Waals

(20) For reviews about multiple additions to fullerenes, see: (a) Thilgen, C.; Sergeyev, S.; Diederich, F. *Top. Curr. Chem.* **2004**, *248*, 1–61. (b) Hirsch, A. *Chem. Rec.* **2005**, *5*, 196–208. (c) Zhou, Z.; Wilson, S. R. *Curr. Org. Chem.* **2005**, *9*, 789–811.

(21) Porphyrin-C_{60} systems connected through a double tether have been studied. See ref 5a and. (a) Armaroli, N.; Marconi, G.; Echegoyen, L.; Bourgeois, J.-P.; Diederich, F. *Chem.—Eur. J.* **2000**, *6*, 1629–1645. (b) Guldi, D. M.; Luo, C.; Prato, M.; Troisi, A.; Zerbetto, F.; Scheloske, M.; Dietel, E.; Bauer, W.; Hirsch, A. *J. Am. Chem. Soc.* **2001**, *123*, 9166–9167.

(22) Phthalocyanine-C_{60} systems connected through a double tether have also been studied. See: (a) Isosomppi, M.; Tkachenko, N. V.; Efimov, A.; Vahasalo, H.; Jukola, J.; Vainiotalo, P.; Lemmetyinen, H. *Chem. Phys. Lett.* **2006**, *430*, 36–40. (b) Niemi, M.; Tkachenko, N. V.; Efimov, A.; Ohkubo, H. K.; Fukuzumi, S.; Lemmetyinen, H. *J. Phys. Chem. A* **2008**, *112*, 6884–6892.

(23) Rapenne, G.; Crassous, J.; Collet, A.; Echegoyen, L.; Diederich, F. *Chem. Commun.* **1999**, 1121–1122.

(24) (a) Reuther, U.; Brandmüller, T.; Donaubauer, W.; Hampel, F.; Hirsch, A. *Chem.—Eur. J.* **2002**, *8*, 2261–2273. (b) Zhou, Z.; Schuster, D. I.; Wilson, S. R. *J. Org. Chem.* **2003**, *68*, 7612–7617. (c) Beuerle, F.; Chronakis, N.; Hirsch, A. *Chem. Commun.* **2005**, 3676–3678. (d) Chronakis, N.; Hirsch, A. *Chem. Commun.* **2005**, 3709–3711.

(25) In general, the DFT-computed energy differences of the two diastereoisomers for each of the regioisomers of **C_{60}-S(-Fc)-*C*α** and **C_{60}-S(-Fc)-*O***, also shown in Figure S17 (only one enantiomer is shown), are not significant, which prevented us from proposing a preferred diastereomeric trisaddition pattern.

(26) Imrie, C.; Loubser, C.; Engelbrecht, P.; McCleland, C. W. *J. Chem. Soc., Perkin Trans. 1* **1999**, 2513–2523.

(27) Echegoyen, L. E.; Djojo, F. D.; Hirsch, A.; Echegoyen, L. *J. Org. Chem.* **2000**, *65*, 4994–5000.

(28) Recent studies have demonstrated the ability of DFT (B3LYP/3-21G*) calculations to describe the geometry and orbital configuration of fullerene-related molecular systems. See: Zandler, M. E.; D'Souza, F. *C. R. Chimie* **2006**, *9*, 960–981.

Table 1. Cyclic Voltammetry Determined Redox Potentials and Radical Ion Pair State Energies of C_{60}−SubPc−Fc (**C_{60}-S-Fc-*C*α** and **C_{60}-S-Fc-*O***) and Reference C_{60}−SubPc (**C_{60}-S-*C*α** and **C_{60}-S-*O***) and SubPc−Fc (**S-Fc-*C*** and **S-Fc-*O***), as well as Reference SubPc (**S-*C*** and **S-*O***), Fc, and C_{60} Derivatives

			S		S-Fc		C_{60}-S		C_{60}-S-Fc	
species	C_{60}	Fc	*-C*	*-O*	*-C*	*-O*	*-C*	*-O*	*-C*	*-O*
					Redox Potentials (V vs Ag/Ag^+)					
C_{60}^{4-}	−1.69						−1.71	−1.67	−1.64	−1.62
$SubPc^{2-}$			−1.48	−1.48	*a*	*a*	*a*	*a*	*a*	*a*
C_{60}^{3-}	−1.46						−1.29	−1.44	−1.39	−1.30
$SubPc^{\bullet-}$			−1.03	−0.92	−1.16	−1.01	−1.07	−1.12	−1.15	−1.09
C_{60}^{2-}	−0.82						*a*	−0.82	−0.93	−0.9
$C_{60}^{\bullet-}$	−0.54						−0.60	−0.63	−0.59	−0.57
$Fc^{\bullet+}$		+0.55			+0.55	+0.51			+0.55	+0.51
$SubPc^{\bullet+}$			+1.03	+1.13	+1.16	+1.10	+1.22	+1.20	+1.24	+1.19
					Radical Ion Pair Energies (eV)					
$Fc^{\bullet+}$−$SubPc^{\bullet-}$					1.71	1.51			1.70	1.60
$SubPc^{\bullet+}$−$C_{60}^{\bullet-}$							1.82	1.83	1.83	1.76
$Fc^{\bullet+}$- SubPc−$C_{60}^{\bullet-}$									1.14	1.08

[a] Difficult to detect.

contact (3.25−3.30 Å) with respect to C_{60}, which explains the low yield of this compound (relative to **C_{60}-S-Fc-*Cβ***), whereas in compound **1O** the distance increases to 3.5−3.6 Å.[29,30]

The small C_{60}−SubPc $\pi-\pi$ distances in **C_{60}-S-Fc-*C*α** and **C_{60}-S-Fc-*O*** lead to rather pronounced electronic interactions between the two redox- and photoactive units, as demonstrated by ground-state electronic absorption and cyclic voltammetry measurements. Both compounds show a broadening and a red-shift of the SubPc *Q*-band when compared to **S-Fc-*C*** and **S-Fc-*O*** or **S-*C*** and **S-*O*** references. This effect is most evident for **C_{60}-S-Fc-*C*α**/**C_{60}-S-*C*α**, which show as well a significant tailing in the red region of the *Q*-band (Figure 3). These features did not change with solvent polarity (i.e., toluene, $CHCl_3$, THF, or benzonitrile) or concentration, so we assume that they are a consequence of the interaction between the closely spaced SubPc and C_{60} π-surfaces.[31]

In cyclic voltammetry measurements (Table 1), SubPcs **S-*C*** and **S-*O*** exhibited amphoteric redox features, that is, cathodic reductions at −1.03 and −0.92 V and anodic oxidations at +1.03 V and +1.13 V (i.e., vs Ag/Ag^+), respectively. On the other hand, the fullerene reference is predominantly active in the direction of the reductive scans, with reduction potentials of −0.54, −0.82, −1.46, and −1.69 V (i.e., vs Ag/Ag^+), while the Fc reference shows only an oxidation step at +0.55 V (i.e., vs Ag/Ag^+).

Significant shifts in the redox features of the different dyads and triads, relative to the aforementioned references, prompt appreciable electronic interactions between the redox active moieties (i.e., electron donor and electron acceptor units). Table 1 demonstrates that these effects are especially pronounced for C_{60}−SubPc (**C_{60}-S-*C*α** and **C_{60}-S-*O***) and C_{60}−SubPc−Fc (**C_{60}-S-Fc-*C*α** and **C_{60}-S-Fc-*O***). In particular, C_{60} reduction in these compounds is rendered appreciably more difficult by approximately 75 ± 25 mV. Please note the overall lack of fullerenes to reflect sensitive electronic interactions. Additionally, the SubPc oxidation indicates the extent of electronic changes. For example, the closer SubPc/C_{60} separation in the **-*C*** series results in larger effects on the first oxidation steps (i.e., 210 ± 10 mV) relative to what has been observed for the **-*O*** series (i.e., 60 ± 10 mV). With these redox parameters in hand, we determined the radical ion pair energies (see Table 1) that support the notion of intramolecular charge separation processes evolving from photoexcited SubPc (see Figure 4).

Excited-State Studies. Fluorescence and Transient Absorption Spectroscopy. SubPcs are versatile chromophores that have been employed as energy donors,[8,32] energy acceptors,[33] electron donors,[8b,f,32] and electron acceptors.[34] They are also strongly emitting fluorophores.[7b] For SubPcs **S-*C*** and **S-*O*** room temperature fluorescence quantum yields of 0.08 ± 0.005 were obtained in this work (see Table 2). From the average between the long-wavelength absorption (i.e., 590 nm) and the short-wavelength fluorescence (i.e., 605 nm) singlet excited-state energies of about 2.0 eV were estimated. These values are in excellent agreement with those established in previously studied SubPc/SubPc−Fc[34a]/SubPc−C_{60}[8] systems. In time-resolved measurements, the SubPc fluorescence was studied by following, for example, the 605 nm maximum as a function of time, and the corresponding profiles were analyzed by fitting them to strictly first-order decay functions. From this fitting procedure lifetimes of 1.60 ± 0.04 ns and 1.70 ± 0.04 ns were determined for **S-*C*** and **S-*O***, respectively. Variation of the solvent polarity between toluene, THF, and benzonitrile did not lead to any appreciable changes in any of the fluorescence attributes (i.e.,

(29) The distance between a benzene dimer in its parallel-displaced configuration has been estimated as 3.6 Å. See, for instance: Sato, T.; Tsuneda, T.; Hirao, K. *J. Chem. Phys.* **2005**, *123*, 104307.

(30) Distances as short as 3.1−3.4 Å have been observed in fullerene host−guest complexes. See: (a) Sygula, A.; Fronczek, F. R.; Sygula, R.; Rabideau, P. W.; Olmstead, M. M. *J. Am. Chem. Soc.* **2007**, *129*, 3842–3843. (b) Gayathri, S. S.; Wielopolski, M.; Pérez, E. M.; Fernández, G.; Sánchez, L.; Viruela, R.; Ortí, E.; Guldi, D. M.; Martín, N. *Angew. Chem., Int. Ed.* **2009**, *48*, 815–819.

(31) (a) Asano, I.; Muranaka, A.; Fukasawa, A.; Hatano, T.; Uchiyama, M.; Kobayashi, N. *J. Am. Chem. Soc.* **2007**, *129*, 4516–4517. (b) Muranaka, A.; Shibahara, M.; Watanabe, M.; Matsumoto, T.; Shinmyozu, T.; Kobayashi, N. *J. Org. Chem.* **2008**, *73*, 9125–9128.

(32) (a) González-Rodríguez, D.; Claessens, C. G.; Torres, T.; Liu, S.-G.; Echegoyen, L.; Vila, N.; Nonell, S. *Chem.—Eur. J.* **2005**, *11*, 3881–3893. (b) Ziessel, R.; Ulrich, G.; Elliott, K. J.; Harriman, A. *Chem.—Eur. J.* **2009**, *15*, 4980–4984.

(33) (a) Camerel, F.; Ulrich, G.; Retailleau, P. *Angew. Chem., Int. Ed.* **2008**, *47*, 8876–8980. (b) Liu, J.-Y.; Yeung, H.-S.; Xu, W.; Li, X.; Ng, D. K. P. *Org. Lett.* **2008**, *10*, 5421–5424.

(34) (a) González-Rodríguez, D.; Torres, T.; Olmstead, M. M.; Rivera, J.; Herranz, M. A.; Echegoyen, L.; Atienza-Castellanos, C.; Guldi, D. M. *J. Am. Chem. Soc.* **2006**, *128*, 10680–10681. (b) El-Khouly, M. E.; Shim, S. H.; Araki, Y.; Ito, O.; Kay, K.-Y. *J. Phys. Chem. B* **2008**, *112*, 3910–3917. (c) Medina, A.; Claessens, C. G.; Rahman, G. M. A.; Lamsabhi, A. M.; Mó, O.; Yáñez, M.; Guldi, D. M.; Torres, T. *Chem. Commun.* **2008**, 1759–1761. (d) El-Khouly, M. E.; Ryu, J. B.; Kay, K.-Y.; Ito, O.; Fukuzumi, S. *J. Phys. Chem. C* **2009**, *113*, 15444–15453.

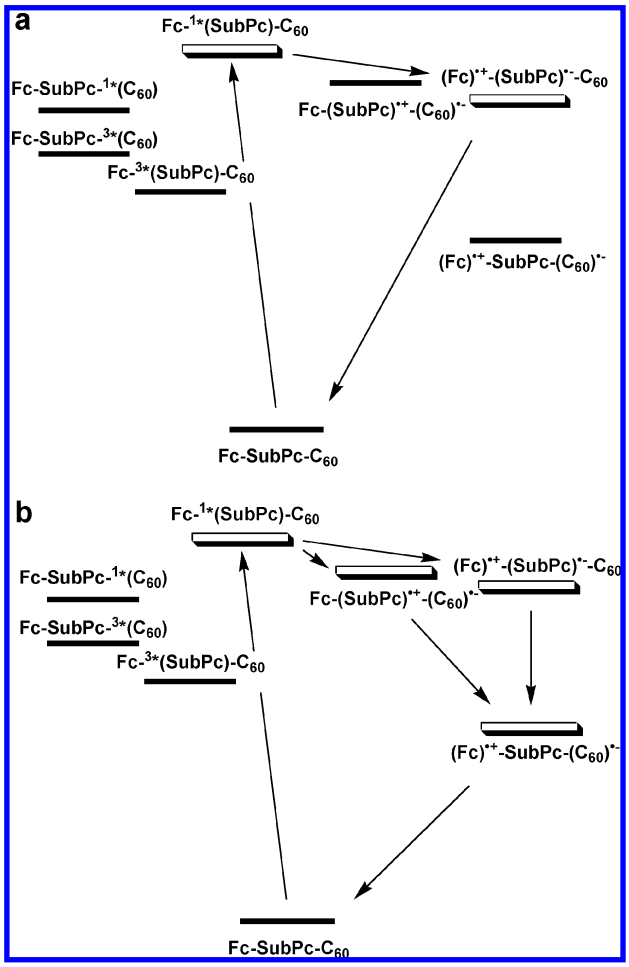

Figure 4. Summary of the photophysical events occurring after SubPc photoexcitation (see discussion below) in (a) **C_{60}-S-Fc-*O***; (b) **C_{60}-S-Fc-*C*α**.

fluorescence quantum yields, fluorescence lifetimes, or fluorescence maxima).

Transient absorption measurements (i.e., femto- and nanosecond resolved) were meant to shed light onto the transient characteristics of the singlet and triplet excited states of SubPcs **S-*C*** and **S-*O***. As can be appreciated from Figure S19, Supporting Information, the strong SubPc fluorescence interferes, on the femtosecond regime (i.e., 0−1500 ps), significantly with the analysis of the singlet excited-state characteristics. Despite this interference, an intersystem crossing rate, converting the strongly emitting singlet excited state to the corresponding triplet manifold, of (6.3 ± 0.2) × 10^8 s^{-1} was obtained. On the contrary, the nanosecond regime (i.e., starting with a time delay of 10 ns) shows clear triplet features that involve transient bleach of the ground-state maximum and a broad transient maximum between 600 and 900 nm; see our previous work.[8a,b,f] The triplet lifetimes are, in THF, 28 μs and comprise quantitative recovery of the singlet ground state.

The presence of the electron-donating ferrocene leads in SubPc−Fc conjugates (**S-Fc-*C*** and **S-Fc-*O***) to substantial quenching of the SubPc fluorescence (Table 2). For **S-Fc-*C*** the quantum yields are 5.8 × 10^{-3}, 4.0 × 10^{-3}, and 1.5 × 10^{-3} in toluene, THF, and benzonitrile, respectively. Slightly stronger is the SubPc fluorescence in **S-Fc-*O***: toluene (3.1 × 10^{-3}), THF (2.1 × 10^{-3}), benzonitrile (0.9 × 10^{-3}). In general, lower quantum yields were detected in the more polar solvents. Notably, a better solvation of charged species in polar media results in (i) lower energies of the radical ion pair states and (ii) larger energy gaps relative to the photoexcited singlet state. Thus, the trend in solvent polarity is attributed to intramolecular charge separation reactions to yield $SubPc^{\bullet-}$−$Fc^{\bullet+}$,[34a] which is mediated through the connecting bridges and facilitated by larger driving forces. Relating the fluorescence quantum yields in the SubPc−Fc hybrids, $\Phi_{(SubPc\text{-}Fc)}$, to that of the SubPc references, $\Phi_{(SubPc)}$, and their lifetimes, $\tau_{(SubPc)}$, helped to determine the rate constants for fluorescence deactivation. Remarkably, the extremely fast rates, especially for **S-Fc-*C*** (i.e., (1.5−5.5) × 10^{10} s^{-1}), as they were derived via this relation, infer a strong coupling between the two moieties. In complementary time-resolved fluorescence measurements, we failed, however, to detect any measurable lifetime that falls within our detection limit (i.e., >100 ps time window).

Next, we turned to transient absorption measurements, following 387 nm excitation. Figure 5 displays a series of new features that develop in parallel with the disappearance of the initially formed SubPc singlet excited state. Implicit here is a very fast singlet excited-state deactivation, vide infra. Particularly, a minimum is seen at 575 nm, which is flanked by a set of maxima at 465 and 615 nm and pronounced shoulders at 495 and 525 nm. In principle, three different pathways for the SubPc singlet excited-state deactivation are feasible. First, a transduction of singlet excited-state energy to ferrocene (2.46 eV), which is, however, thermodynamically unfeasible. By contrast, the low-lying nature of the ferrocene triplet excited state (1.64 eV) opens, in principle, the opportunity for the second pathway, namely an energy transfer, however, only in form of a singlet−triplet transfer. But the weak triplet−triplet characteristics are markedly different from those noted. In fact, earlier

Table 2. Photophysical Parameters for C_{60}−SubPc−Fc (**C_{60}-S-Fc-*C*α** and **C_{60}-S-Fc-*O***) and Reference C_{60}−SubPc (**C_{60}-S-*C*α** and **C_{60}-S-*O***) and SubPc−Fc (**S-Fc-*C*** and **S-Fc-*O***), as well as Reference SubPc Derivatives (**S-*C*** and **S-*O***)

		S		S-Fc		C_{60}-S		C_{60}-S-Fc	
	solvent	*-C*	*-O*	*-C*	*-O*	*-C*	*-O*	*-C*	*-O*
Φ^a	toluene	0.08	0.08	5.8 × 10^{-3}	3.1 × 10^{-3}	5.8 × 10^{-4}	8.5 × 10^{-4}	6.1 × 10^{-4}	5.5 × 10^{-3}
	THF	0.081	0.081	4.0 × 10^{-3}	2.1 × 10^{-3}	5.2 × 10^{-4}	7.3 × 10^{-4}	5.0 × 10^{-4}	4.9 × 10^{-3}
	BzCN	0.079	0.079	1.5 × 10^{-3}	9.0 × 10^{-4}	3.9 × 10^{-4}	6.2 × 10^{-4}	4.0 × 10^{-4}	1.0 × 10^{-3}
Φ^b	toluene						8.0 × 10^{-4}		
	THF						6.2 × 10^{-4}		
	BzCN						5.7 × 10^{-4}		
τ [ns]^a	THF	1.6	1.7	<0.1	<0.1	<0.1	<0.1	<0.1	<0.1
τ [ns]^b	THF						1.7		
k_{CS} [s^{-1}]	THF			9.5 × 10^{10}	1.9 × 10^{11}	1.5 × 10^{11}	1.5 × 10^{11} [c]	2.1 × 10^{11}	1.8 × 10^{11}
k_{CR} [s^{-1}]	THF			7.4 × 10^6	9.4 × 10^6	1.0 × 10^7		1.1 × 10^4	

[a] SubPc fluorescence. [b] C_{60} fluorescence. [c] Energy transfer.

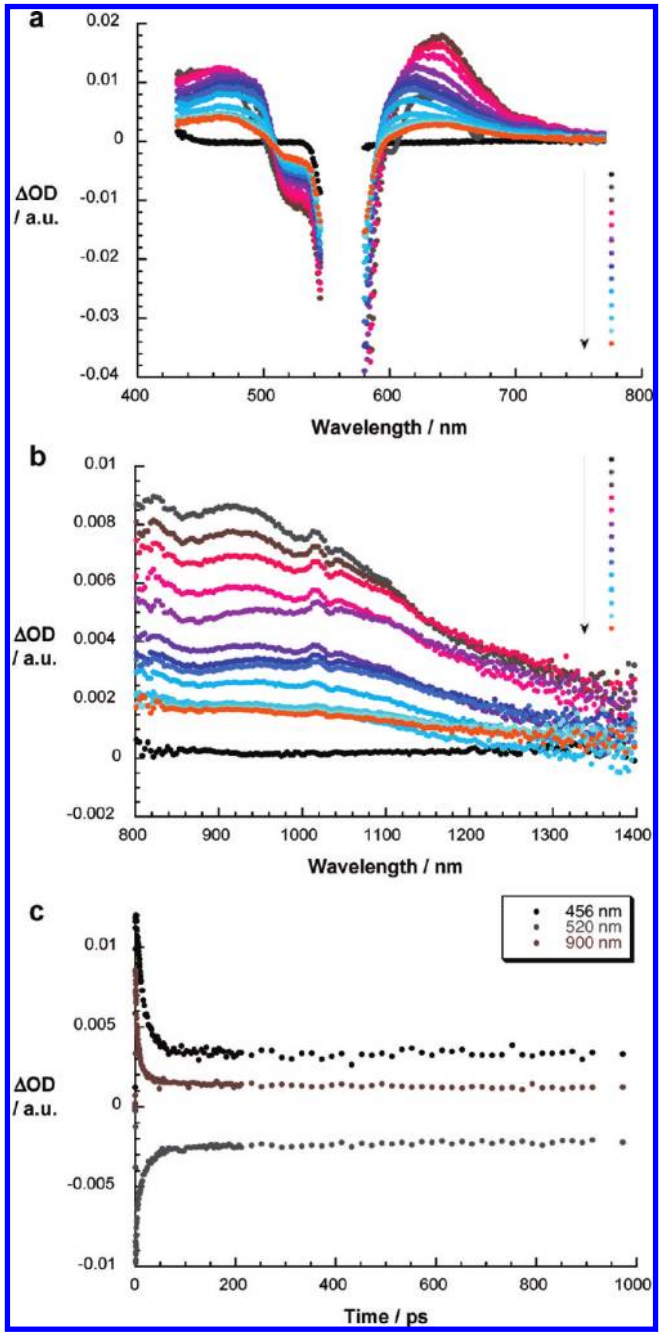

Figure 5. (a) Differential absorption spectra (visible) obtained upon femtosecond flash photolysis (550 nm, 150 nJ) of **S-Fc-*C*** in THF with several time delays between 0 and 100 ps at room temperature; see figure legend for time evolution. (b) Differential absorption spectra (near-infrared) obtained upon femtosecond flash photolysis (550 nm, 150 nJ) of **S-Fc-*C*** in THF with several time delays between 0 and 100 ps at room temperature; see figure legend for time evolution. (c) Time−absorption profiles of the spectra at 456, 520, and 900 nm, monitoring the charge separation dynamics.

extinction coefficients of less than 500 M^{-1} cm^{-1} were estimated, using laser flash photolysis, for the triplet−triplet absorption in the visible region. This leaves essentially the third pathway, charge separation to yield $SubPc^{\bullet -}-Fc^{\bullet +}$, as the only responsible channel for the singlet excited-state deactivation.

Time−absorption profiles for SubPc−Fc **S-Fc-*C*** in THF (i.e., 456, 520, and 900 nm), as shown in Figure 5, illustrate the charge separation dynamics. Kinetic analysis of these time−absorption profiles gives rise to a very fast decay rate constant, 9.5×10^{10} s^{-1}. Please note that the decay rate for **S-Fc-*O*** is, in line with the

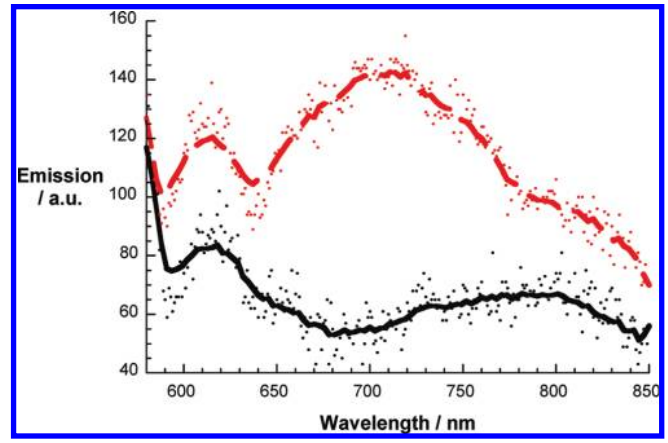

Figure 6. Room temperature steady-state fluorescence spectra of **C_{60}-S-*C*α** (black spectrum) and **C_{60}-S-*O*** (red spectrum) in THF upon 560 nm excitation.

trends seen in the steady-state fluorescence and electrochemical experiments, somewhat faster (i.e., 1.9×10^{11} s^{-1}).

The $SubPc^{\bullet -}-Fc^{\bullet +}$ radical ion pair state[34a] is stable on the time scale of our femtosecond experiments, that is, up 3 ns. When complementing these femtosecond experiments with nanosecond resolved experiments, the $SubPc^{\bullet -}-Fc^{\bullet +}$ features (see Figure S20, Supporting Information) started slowly to vanish. The decays were monoexponential and afforded lifetimes in THF of 135 ns (7.4×10^6 s^{-1}) and 106 ns (9.4×10^6 s^{-1}), for **S-Fc-*C*** and **S-Fc-*O***, respectively.

When analyzing the fluorescence spectra of the C_{60}−SubPc trisadducts (**C_{60}-S-*C*α** and **C_{60}-S-*O***), a trend toward much stronger fluorescence quenching, relative to what was seen for SubPc−Fc, is evident. For example, in THF the quantum yields are 5.2×10^{-4} and 7.3×10^{-4}, for **C_{60}-S-*C*α** and **C_{60}-S-*O***, respectively. From this we conclude that the interactions within the C_{60}−SubPc systems must be stronger than within the SubPc−Fc systems. This conclusion is further supported by the rate constants of SubPc singlet excited-state deactivation of 9.5×10^{10} s^{-1} (**C_{60}-S-*C*α**) and 6.7×10^{10} s^{-1} (**C_{60}-S-*O***) in THF. Similarly to SubPc−Fc compounds **S-Fc-*C*** and **S-Fc-*O***, fluorescence lifetime measurements with C_{60}−SubPc **C_{60}-S-*C*α** and **C_{60}-S-*O*** failed in terms of registering any detectable SubPc fluorescence.

A closer analysis of the fluorescence spectra (see Figure 6) reveals for **C_{60}-S-*O***, besides the strongly quenched SubPc fluorescence in the 580−650 nm range, the familiar C_{60} fluorescence in the red (i.e., 650−850 nm). The C_{60} fluorescence quantum yields, which are about $8.0 \pm 0.2 \times 10^{-4}$ in toluene, THF, and benzonitrile, suggest a quantitative transduction of singlet excited-state energy from SubPc (i.e., 2.0 eV) to C_{60} (i.e., ca. 1.7 eV).[35] A similar reactivity has been previously reported for several SubPc-C_{60} systems.[8b,f] On the contrary, for SubPc-C_{60} **C_{60}-S-*C*α** the lack of C_{60} fluorescence implies a different reactivity, namely charge separation to form the one-electron-reduced C_{60} radical anion and the one-electron-oxidized SubPc radical cation. The shorter SubPc/C_{60} distance in **C_{60}-S-*C*α** leads to a notable perturbation of the electronic structure for both components in the ground state, as evidenced, for example, in the absorption spectra. A reasonable rationale implies a partial shift of electron transfer density. Consequently, we postulate that

(35) In fluorescence lifetime measurements a lifetime of 1.7 ns was registered for the C_{60} fluorescence.

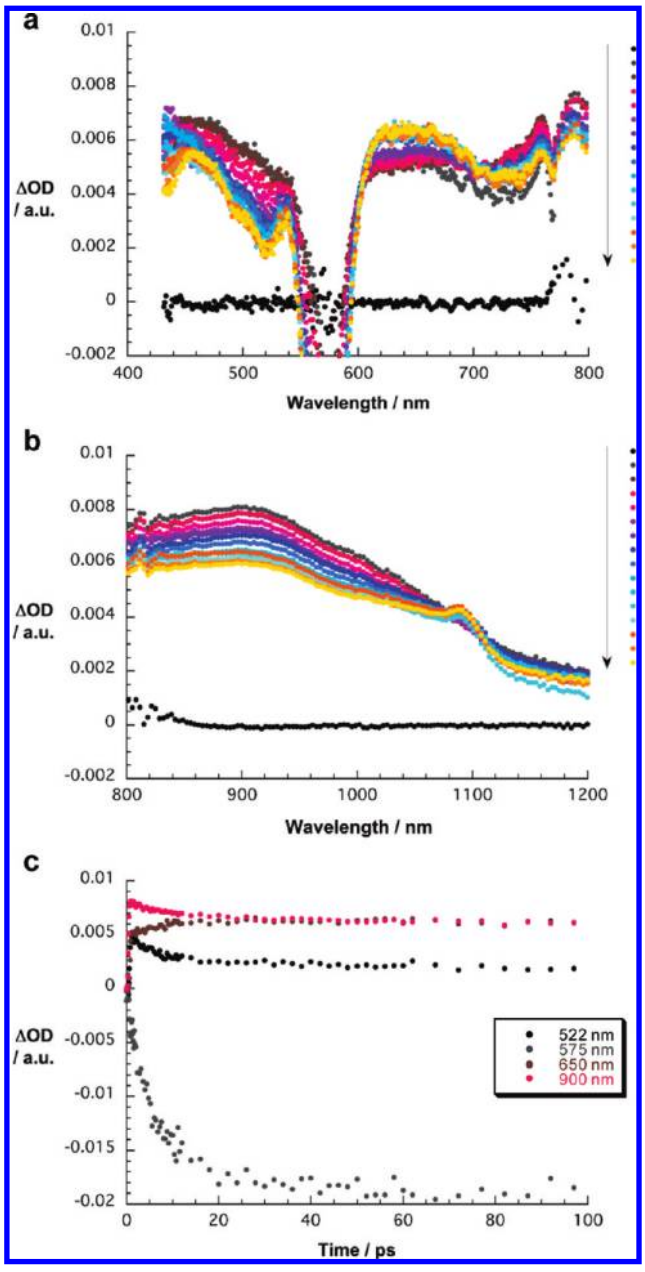

Figure 7. (a) Differential absorption spectra (visible) obtained upon femtosecond flash photolysis (550 nm, 150 nJ) of **C_{60}-S-*C*α** in THF with several time delays between 0 and 100 ps at room temperature; see figure legend for time evolution. (b) Differential absorption spectra (near-infrared) obtained upon femtosecond flash photolysis (550 nm, 150 nJ) of **C_{60}-S-*C*α** in THF with several time delays between 0 and 100 ps at room temperature; see figure legend for time evolution. (c) Time−absorption profiles of the spectra at 522, 575, 650, and 900 nm, monitoring the charge separation dynamics.

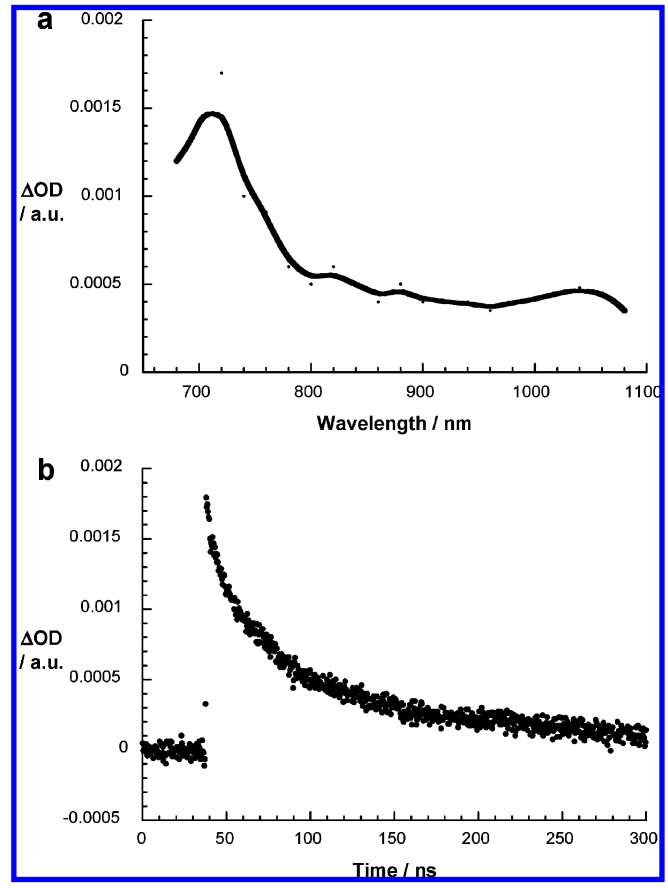

Figure 8. (a) Differential absorption spectrum (near-infrared) obtained upon nanosecond flash photolysis (535 nm, 150 nJ) of **C_{60}-S-*C*α** in THF with a time delay of 25 ns at room temperature. (b) Time−absorption profiles of the spectra at 720 nm, monitoring the charge recombination dynamics.

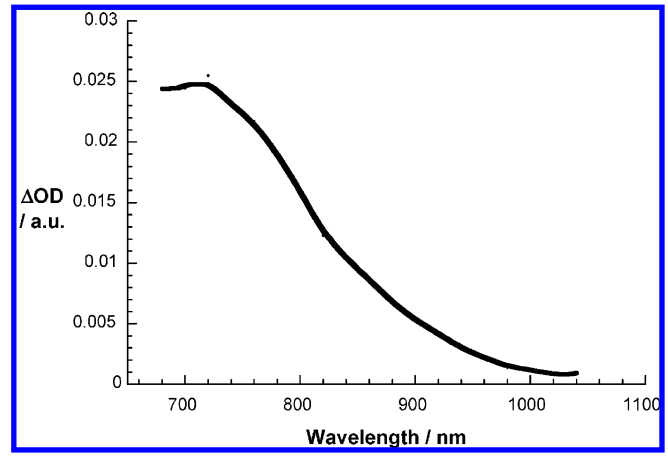

Figure 9. Differential absorption spectrum (near-infrared) obtained upon nanosecond flash photolysis (535 nm, 150 nJ) of **C_{60}-S-*O*** in THF with a time delay of 25 ns at room temperature.

in this preactivated state charge separation is favored over energy transfer. In the case of larger SubPc/C_{60} distances, as in **C_{60}-S-*O***, weaker or no ground-state interactions result in a dominant energy transfer deactivation (see Figure 4).[9]

The transient absorption changes monitored for **C_{60}-S-*C*α** are substantially different from the aforementioned cases (i.e., **S-Fc-*C*** and **S-Fc-*O***); please compare Figures 5 and 7. Overall the transient features are much broader. In addition, peaks at 460, 540, and 660 nm evolve from the transformation of the initially formed SubPc singlet excited state into the photoproduct. Since the spectra do not resemble any excited-state characteristics (i.e., SubPc triplet, C_{60} singlet, or C_{60} triplet), we assign the new features to those of the $C_{60}^{\bullet-}$−$SubPc^{\bullet+}$ radical ion pair state; see our previous work.[8b,f] Further support for this assumption is shown in Figure 8. In particular, the $C_{60}^{\bullet-}$−$SubPc^{\bullet+}$ radical ion pair shows the characteristic fingerprint of the one-electron reduced C_{60} radical anion around 1080 nm. From the time-absorption profiles an intramolecular rate constant of 1.5×10^{11} s^{-1} was derived in THF, which is in good agreement with the steady-state fluorescence experiments. As Figure 8

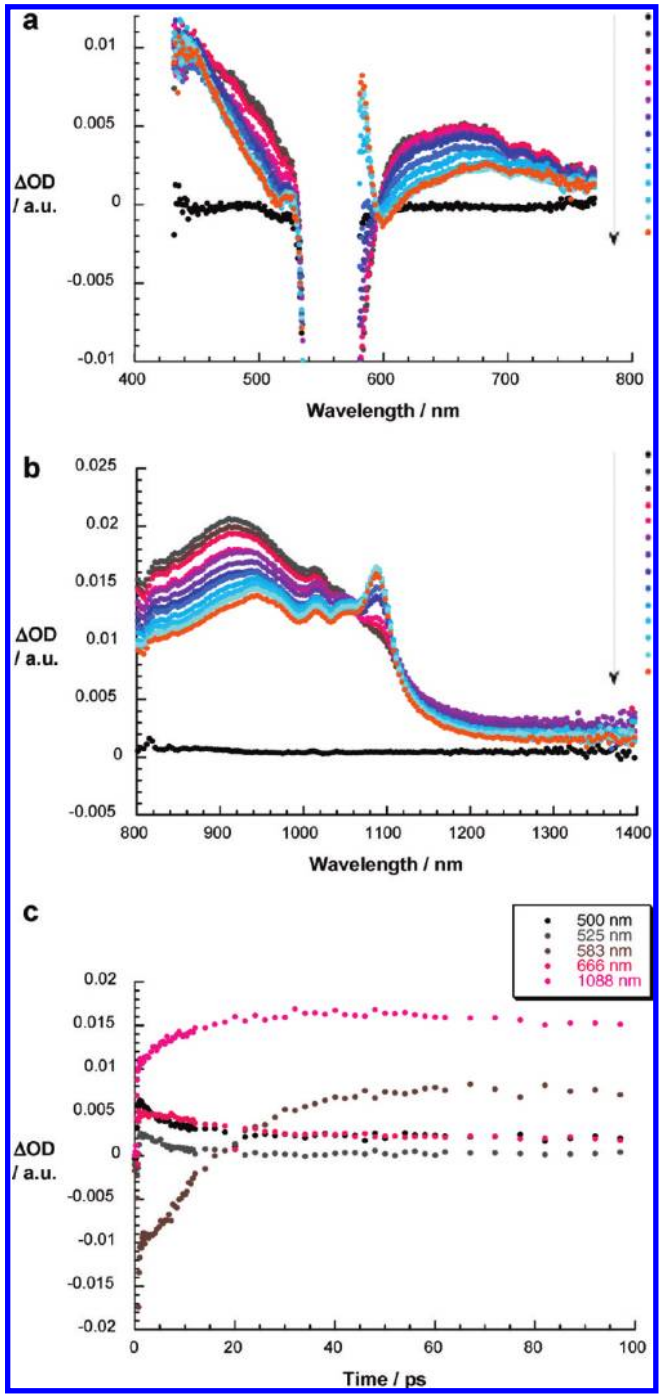

Figure 10. (a) Differential absorption spectra (visible) obtained upon femtosecond flash photolysis (550 nm, 150 nJ) of **C_{60}-S-Fc-*C*α** in THF with several time delays between 0 and 100 ps at room temperature; see figure legend for time evolution. (b) Differential absorption spectra (near-infrared) obtained upon femtosecond flash photolysis (550 nm, 150 nJ) of **C_{60}-S-Fc-*C*α** in THF with several time delays between 0 and 100 ps at room temperature; see figure legend for time evolution. (c) Time-absorption profiles of the spectra at 500, 525, 583, 666, and 1088 nm, monitoring the charge separation dynamics.

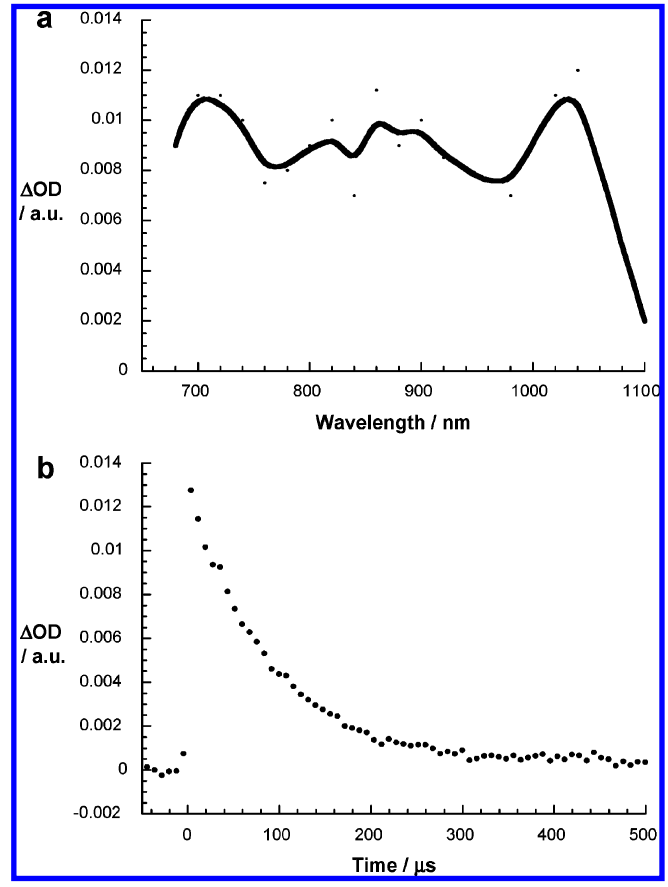

Figure 11. (a) Differential absorption spectrum (near-infrared) obtained upon nanosecond flash photolysis (535 nm, 150 nJ) of **C_{60}-S-Fc-*C*α** in THF with a time delay of 25 ns at room temperature. (b) Time−absorption profiles of the spectra at 1060 nm, monitoring the charge recombination dynamics.

demonstrates, the $C_{60}^{\bullet-}$−$SubPc^{\bullet+}$ is surprisingly stable on our femtosecond time scale (i.e., up 3 ns) and starts to decay on the nanosecond time scale (i.e., starting at 8 ns). In THF, a remarkable lifetime of 97 ns (1.0×10^7 s^{-1}) was noted for **C_{60}-S-*C*α**.

As indicated above, the photoreactivity of **C_{60}-S-*O*** is different, and hence on the nanosecond time scale, the only detectable product is the long-lived SubPc triplet excited state (Figure 9). The mechanism for converting the initially formed SubPc singlet excited state into the final SubPc triplet excited state is a cascade of energy transfer processes with rates of 1.5×10^{11} s^{-1} (i.e., singlet−singlet energy transfer), 6.3×10^8 s^{-1} (i.e., intersystem crossing), and $\gg 6.3 \times 10^8$ s^{-1} (i.e., triplet−triplet energy transfer); see our previous work.[8b,f]

When comparing C_{60}−SubPc **C_{60}-S-*C*α** and C_{60}−SubPc−Fc **C_{60}-S-Fc-*C*α**, the same extend of SubPc fluorescence quenching is noted, suggesting a similar SubPc deactivation. On the other hand, if we now compare **C_{60}-S-Fc-*O*** and **C_{60}-S-*O***, the C_{60}−SubPc−Fc conjugate shows no detectable C_{60} fluorescence and gives rise to a slightly stronger SubPc fluorescence than that of the C_{60}−SubPc conjugate.[36] In THF, for example, the quantum yield is 4.9×10^{-3}. This surprising result suggests that the deactivation in **C_{60}-S-Fc-*O*** is, at least in part, governed through ferrocene. In fact, we will demonstrate below that the C_{60}−$SubPc^{\bullet-}$−$Fc^{\bullet+}$ species is formed.

Differential absorption changes, following the femtosecond laser excitation of **C_{60}-S-Fc-*C*α**, are best described as superimposable to those seen for **C_{60}-S-*C*α**. Here, please compare Figures 7 and 10. Kinetically the results are also identical: SubPc singlet decays of 2.1×10^{11} s^{-1} for **C_{60}-S-Fc-*C*α** and 1.5×10^{11} s^{-1} for **C_{60}-S-*C*α**. The presence of (i) ferrocene and (ii) a

(36) No measurable C_{60} fluorescence was registered in time-resolved experiments.

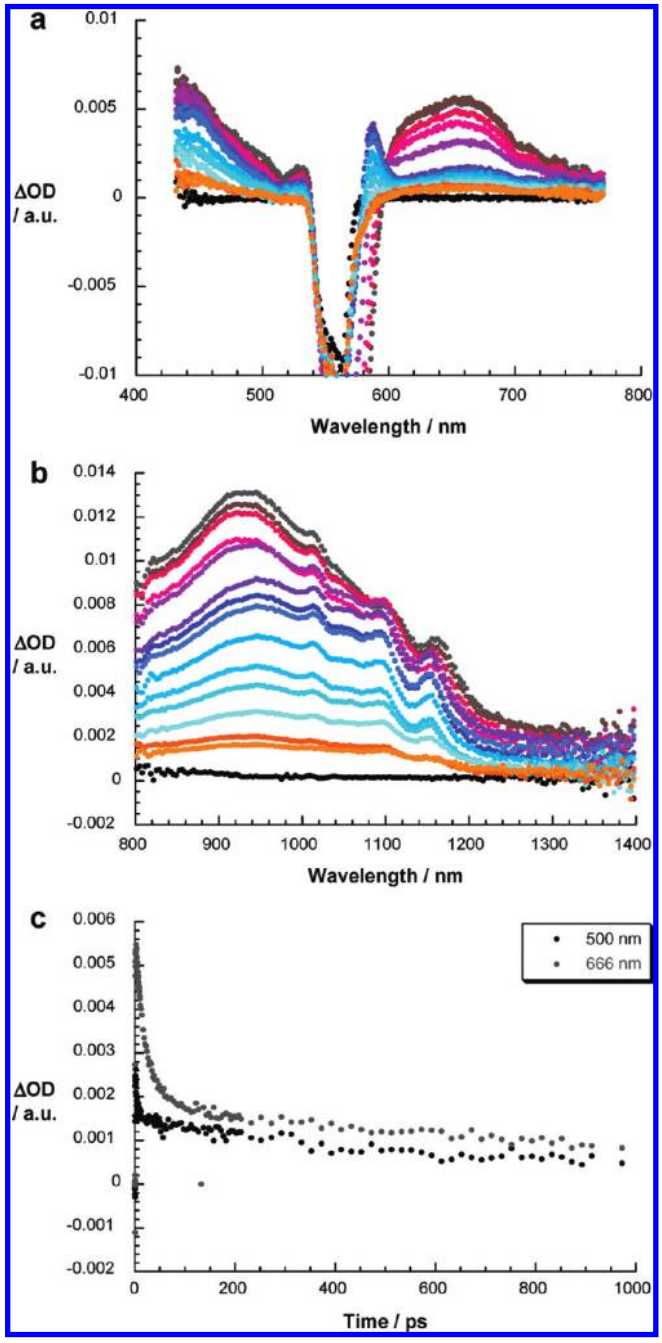

Figure 12. (a) Differential absorption spectra (visible) obtained upon femtosecond flash photolysis (550 nm, 150 nJ) of **C_{60}-S-Fc-*O*** in THF with several time delays between 0 and 1000 ps at room temperature; time evolution from black to red to blue and orange. (b) Differential absorption spectra (near-infrared) obtained upon femtosecond flash photolysis (550 nm, 150 nJ) of **C_{60}-S-Fc-*O*** in THF with several time delays between 0 and 1000 ps at room temperature; time evolution from black to red to blue and orange. (c) Time-absorption profiles of the spectra at 500 and 666 nm, monitoring the charge separation dynamics.

significant driving force for a subsequent charge shift reaction[37] in **C_{60}-S-Fc-*C*α**, leads to the expected $C_{60}^{\bullet-}$−$SubPc^{\bullet+}$−Fc/ $C_{60}^{\bullet-}$−SubPc−$Fc^{\bullet+}$ transformation with a rate constant of 1.6×10^9 s^{-1}. Nevertheless, we noticed, in addition, the formation of the 525 and 590 nm markers for C_{60}−$SubPc^{\bullet-}$−$Fc^{\bullet+}$,[34a] which transforms with 1.0×10^9 s^{-1} to the same $C_{60}^{\bullet-}$−$SubPc$−$Fc^{\bullet+}$ photoproduct that was formed via the $C_{60}^{\bullet-}$−$SubPc^{\bullet+}$−Fc intermediate (see Figure 4). In line with the aforementioned description, we see a nanosecond spectrum that only bears the characteristics of the one-electron reduced C_{60} radical anion (see Figure 11) since the features associated with the one-electron-oxidized ferrocene are simply too weak to be detected. More precisely, the low extinction coefficient of ∼500 M^{-1} cm^{-1} at 625 nm is masked by the much stronger absorption (i.e., >5000 M^{-1} cm^{-1}) of $C_{60}^{\bullet-}$ in this region. The $C_{60}^{\bullet-}$−$SubPc$−$Fc^{\bullet+}$ decay in **C_{60}-S-Fc-*C*α** is monoexponential and its analysis leads to a remarkable lifetime of 94 μs (1.1×10^4 s^{-1}), which is 3 orders of magnitude higher than in **C_{60}-S-*C*α**. The quantitative product of the charge recombination is the C_{60}−SubPc−Fc singlet ground state.

Let us finally direct our attention to **C_{60}-S-Fc-*O***. Initially following the photoexcitation, differential absorption changes suggest a charge separation that involves C_{60}−$SubPc^{\bullet-}$−$Fc^{\bullet+}$; see Figure 12. In particular, we see the 525 and 590 nm markers. In other words, the reaction is similar to what has been concluded for SubPc−Fc **S-Fc-*O***. Then, the lack of coupling between SubPc and C_{60}, which already resulted for **C_{60}-S-*O*** in an all energy transfer scenario, prevents a subsequent charge shift reaction (i.e., forming the $C_{60}^{\bullet-}$−SubPc−$Fc^{\bullet+}$ species as observed for **C_{60}-S-Fc-*C*α**). In line with this conclusion, we see on the nanosecond time scale a spectrum that resembles the SubPc triplet excited state (not shown). Also the C_{60}−$SubPc^{\bullet-}$−$Fc^{\bullet+}$ radical ion pair state lifetime (i.e., 92 ns, 1.1×10^7 s^{-1}) in **C_{60}-S-Fc-*O*** is comparable to that found in **S-Fc-*O***. In addition, we noticed the sequence of energy transfer reactions as a competitive deactivation path in **C_{60}-S-Fc-*O*** at which end the long-lived SubPc triplet excited state remains.

Conclusions

The concave side of SubPcs is ideally suited to cover a large surface of C_{60}, thus potentially affording a high degree of orbital overlap between the two π-conjugated molecules. In order to impose a strong interchromophore interaction, we have designed a system with restricted flexibility by a three-point anchoring, via Bingel trisaddition reaction, of the C_3-symmetrical SubPc macrocycle to C_{60}. On the other hand, the distance between the two components, and hence the degree of orbital overlap, could be finely adjusted by making small changes in the semirigid spacer. Just varying the linkage to the SubPc macrocycle from a C−C bond to a C−O−C bond can strongly influence not just the regioselectivity of the trisaddition reaction but also the distance and degree of interaction between the two π-surfaces in the final products. As a consequence, only when the C_{60} and SubPc units are held at a close distance and exhibit a high degree of electronic interactions is a sequential electron transfer process triggered, ultimately leading to the long-lived (∼0.1 ms), spatially separated $C_{60}^{\bullet-}$−SubPc−$Fc^{\bullet+}$ radical ion pair. Our results shed light on the subtle interplay between different photophysical mechanisms operating between π-conjugated, electronically active molecules that are confined at intimate van der Waals contact.

Acknowledgment. This work is dedicated to Professor Dr. Dr. h.c. Michael Hanack on the occasion of his 80th birthday. This work has been supported by the COST Action D35, and the EU Project ROBUST DSC, FP7-Energy-2007-1-RTD, no. 212792. Financial support by the MEC, Spain (CTQ2008-00418/BQU, CONSOLIDER-INGENIO 2010 CDS 2007-00010, PLE2009-

(37) Charge shift reactions involving SubPc and C_{60} have also been observed in SubPc−triphenylamine−C_{60} triads. See ref 34b.

0070), and CAM (MADRISOLAR-2, S2009/PPQ/1533), is gratefully acknowledged. This work was also supported by the Deutsche Forschungsgemeinschaft through SFB583, DFG (GU 517/4-1), FCI, and the Office of Basic Energy Sciences of the U.S. Department of Energy. D.G.R. acknowledges a Marie Curie Reintegration Grant (230964).

Supporting Information Available: Experimental section, synthetic procedures, characterization data, and some selected supplementary figures. This material is available free of charge via the Internet at http://pubs.acs.org.

JA105864R